JM PAPERS

Longitudinal wall motion during peristalsis and its effect on reflux

Kourosh Kalayeh[1],[†], **Haotian Xie**[2]**, J. Brian Fowlkes**[3]**, Bryan S. Sack**[1] **and William W. Schultz**[2]

[1]Department of Urology, University of Michigan, Ann Arbor, MI 48109, USA

[2]Department of Mechanical Engineering, University of Michigan, Ann Arbor, MI 48109, USA

[3]Department of Radiology, University of Michigan, Ann Arbor, MI 48109, USA

In this study, for the first time, we consider longitudinal motion of the walls during peristalsis in a distensible tube and how this affects backward (or retrograde) flow, i.e. peristaltic reflux. Building on the analytical model developed by Shapiro *et al.* (*J. Fluid Mech.*, vol. 37, no. 4, 1969, pp. 799–825) based on lubrication theory, we model peristalsis as a two-dimensional infinite sinusoidal wavetrain. We develop an objective function with high mechanical pumping efficiency and low reflux to find optimal peristalsis conditions. We show that optimal wall longitudinal motion contributes substantially to limiting reflux during peristalsis. The results suggest that the optimal form of wall longitudinal velocity is a linear function of the wall transverse coordinate, moving forward with the wave when the tube is distended and retracting when contracted. Our results are in general agreement with clinical observations of ureteral peristalsis.

1. Introduction

Peristalsis is a form of fluid transport caused by a propagation of progressive wave of dilatation and contraction along the length of a distensible tube. While peristalsis is a topic of interest in many areas with physiological (e.g. urinary tract, gastro-intestinal tract, etc.) and non-physiological (e.g. roller pumps) applications, our main motivation here is driven by the need to understand ureteral peristalsis and its effect on urinary reflux, which might result in urine stasis leading to urinary tract infections (UTIs).

† Email address for correspondence: kouroshm@umich.edu

Ureteral peristalsis is believed to be the main mechanism transporting urine from the kidneys to the bladder (Weiss 1978). Although, ureteral peristalsis is not well understood (Kiil 1973; Vahidi *et al.* 2011), the general consensus is that the ureteral lumen (the hollow inner volume of the ureter) narrows due to contraction of circular muscles while at the same time it shortens due to contraction of longitudinal muscles (Kiil 1973). Under normal conditions, the bolus of urine formed between two consecutive constricted locations of a wave is propelled towards the bladder, where it goes through the ureteral valve known as the ureterovesical junction (UVJ) (Kalayeh *et al.* 2020). While peristaltic reflux, in general, is harmless (Boyarsky & Labay 1981), it increases the probability of UTIs with potential transmission of bacteria from the bladder to the kidneys, secondary to increased urinary stasis. This is especially true when peristaltic reflux accompanies UVJ deficiency, resulting in retrograde flow of the urine from the bladder to the ureters which is known as vesicoureteral reflux (VUR) (Kalayeh *et al.* 2021). Under such conditions, peristaltic reflux facilitates passage of bacteria in the bladder to the kidneys, resulting in UTIs. Jörgensen & Stödkilde-Jörgensen (1985) and Jörgensen (1985, 1986) suggest that ureteral peristalsis might be one of the VUR prevention mechanisms.

The pioneering work modelling peristalsis of Shapiro (1967) is the basis of many models that followed. This study and its extensions (Shapiro, Jaffrin & Weinberg 1969; Jaffrin & Shapiro 1971; Weinberg, Eckstein & Shapiro 1971) consider peristalsis as a two-dimensional and/or axisymmetric infinite train of sinusoidal waves (therefore, periodic boundary conditions) for negligible Reynolds numbers. These assumptions enable use of lubrication theory (Som, Biswas & Chakraborty 2011). Alternatively, Fung & Yih (1968) solve the problem of peristalsis based on a small peristaltic amplitude assumption. This is not consistent with clinical observations (Woodburne & Lapides 1972), where it has been shown that during the constriction phase of peristalsis the ureter is almost fully closed (i.e. large peristaltic amplitudes). Additionally, they analyse reflux with an Eulerian description that, as shown by Shapiro & Jaffrin (1971), is not correct. This will be further discussed below, when we analyse peristaltic reflux.

Lykoudis & Roos (1970) argue that pressure profiles obtained with sinusoidal waveforms do not match those observed during ureteral peristalsis; hence, they solve an inverse problem to find an appropriate waveform. However, they fail to provide their waveform and inexplicably zero out negative pressures (their figure 2). Later, Manton (1975) extends the analysis of Lykoudis & Roos (1970) to include effects of small Reynolds numbers. They provide the waveform expression of Lykoudis & Roos (1970), but they do not provide and compare corresponding pressure profiles.

Liron (1976) focuses on the mechanical efficiency of peristalsis while expanding in wave and Reynolds numbers and considers two additional non-physiological waveforms: 'plow form' and 'nipple form'. Takabatake & Ayukawa (1982) solve the full Navier–Stokes equations using finite differences and, hence, lift the simplifying assumptions on the magnitudes of wave amplitude, wavelength and Reynolds number. These models are extensions to the Shapiro *et al.* (1969) model without significantly improving that model in terms of the general functionality of peristalsis as a physiological flow and its effect on reflux.

Li & Brasseur (1993) generalize the classical lubrication-theory model of peristalsis to arbitrary wave shape and wavenumber in tubes of finite length. Therefore, they solve an unsteady problem. This is also of interest when considering the inter-'ends' (i.e. the kidney and bladder) effects that require non-periodic boundary conditions. More recently the problem of peristalsis has been solved numerically (Hosseini *et al.* 2018; Razavi & Jouybar 2018; Mancha Sánchez *et al.* 2020; Keni *et al.* 2021), addressing different

clinical scenarios. All of these numerical models generally confirm the applicability of lubrication theory in analysing ureteral peristalsis.

Histological studies showing the presence of longitudinal and circumferential ureteral smooth muscles (Mackinnon *et al.* 1970), animal studies on the ureter kinematics during peristalsis with 'quick freezing' (Woodburne & Lapides 1972), videomicroscopy (Osman *et al.* 2009) and surgical observations confirm that during peristalsis the ureter not only moves transversely but also longitudinally. This requires that the inner wall of the ureter moves in an orbital, cyclic fashion during peristalsis.

The work presented here, for the first time, considers longitudinal motion of the wall in modelling peristalsis. We will show that longitudinal motion of the ureteral wall during peristalsis is crucial for reflux suppression in the ureter.

2. Model development

We follow Shapiro *et al.* (1969) with a change in boundary conditions to include longitudinal wall motion in the lubrication model for peristalsis. We also adopt the regularly assumed two-dimensional planar flow to qualitatively model peristalsis. However, axisymmetric modelling is also only qualitative as the constricted cross-section is far from axisymmetric (Woodburne & Lapides 1972). Hence, we choose the simpler alternative that allows comparison to previous modelling results.

In terms of nomenclature, we note the following. While Shapiro *et al.* (1969) start their analysis with dimensional variables and then non-dimensionalize, we start with non-dimensional variables, with the ˆ symbol indicating dimensional quantities. Furthermore, for a peristaltic amplitude (ϕ in Shapiro *et al.* (1969) and b here) and reflux fraction ($\mathscr{R}$ in Shapiro *et al.* (1969) and $\mathcal{X}$ here), we use different variable names. Finally, capital letters signify variables in the laboratory (unsteady) frame of reference, while small letters represent variables in the wave (steady) frame of reference (see Appendices A and B for more details on the solution development and computation hardware).

2.1. *Problem formulation*

The model developed in Shapiro *et al.* (1969) is based on lubrication theory. More specifically, the following assumptions have been made.

(i) Planar geometry: it is assumed that ureteral peristalsis is planar and can be qualitatively modelled by two-dimensional geometry.

(ii) Long wavelength: it is assumed that the peristaltic wavelength is much larger than the lumen height, a necessary condition for applicability of lubrication theory. This is justified by the anatomy of the ureter in a typical adult person as noted in table 1.

(iii) Inertia-free flow: the Reynolds number is assumed to be sufficiently small.

(iv) Fluid properties: the fluid is assumed to be Newtonian with constant density and viscosity.

(v) Infinite sinusoidal wavetrain: the flow is periodic and the peristaltic wave is assumed to be an infinite progressive train of sinusoidal waves, moving longitudinally at a constant velocity. The more realistic peristaltic waveform described by Lykoudis & Roos (1970) is eschewed in favour of simplicity and comparison to the majority of previous studies. Also, the periodic boundary condition assumed here is challenged for a small number of waves as pointed out by Li & Brasseur (1993).

Length	$\hat{L} \approx 22$ to 30 cm
Lumen height	$2\hat{a} \approx 1$ to 6 mm
Peristaltic wavelength	$\hat{\lambda} \approx 6$ to 10 cm
Peristaltic wave travelling velocity	$\hat{c} = 2$ to 3 cm s^{-1}

Table 1. Normal anatomical information of a typical ureter and peristalsis in an adult person (Zheng *et al.* 2021).
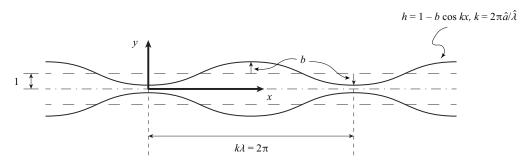

Figure 1. A schematic of a peristalsis wave in the wave frame (moving left to right with the peristalsis wave) with non-dimensional variables. The dashed lines represent peristalsis of zero amplitude ($b = 0$). The dashed-dotted line is the symmetry plane.

Using standard non-dimensionalization, we set the wave velocity c, fluid viscosity μ and lumen half-height a to unity (see Appendix C for more detail). In the laboratory frame the problem is unsteady and the wall transverse coordinate H is given by

$$H = 1 - b\cos(kX - \omega t), \tag{2.1}$$

where b is the peristaltic amplitude, X is the longitudinal coordinate in the laboratory frame, t is time, $k = 2\pi/\lambda$ is the wavenumber, $\omega = 2\pi/T$ is the angular frequency and T is the waveperiod. The lubrication approximation is valid for small normalized wavenumbers, $k \ll 1$. Attaching the frame of reference to the travelling wave and assuming the pressure gradient between the 'ends' (i.e. the bladder and kidney) remains constant (i.e. assuming periodic boundary conditions), the flow becomes steady, and the wall transverse coordinate becomes

$$h = 1 - b\cos kx. \tag{2.2}$$

The transformation between the two frames is given by

$$\left.\begin{aligned} x = X - t, \quad y = Y, \\ u(x, y) = U(X - t, Y) - 1, \quad v(x, y) = V(X - t, Y), \end{aligned}\right\} \tag{2.3}$$

where (x, y) and (X, Y) are parameterizing longitudinal and transverse coordinates in the wave and laboratory frames of reference, respectively. Similarly, (u, v) and (U, V) are longitudinal and transverse velocity components in the wave and laboratory frames of reference. A schematic of a peristalsis wave, as described above, in the steady frame of reference with non-dimensional variables is shown in figure 1.

964 A30-4

With the lubrication assumptions, the Navier–Stokes equation in the longitudinal and transverse directions becomes

$$\frac{\partial p}{\partial x} = \frac{\partial^2 u}{\partial y^2}, \quad \frac{\partial p}{\partial y} = 0. \tag{2.4a,b}$$

To account for wall longitudinal motion, we set $u(y = h) = -1 + \beta(x)$, where $\beta(x)$ is a 2π-periodic function in space and time (in the Lagrangian sense). Note that $\beta = 0$ recovers the Shapiro *et al.* (1969) solution. Therefore, the boundary conditions become

$$\left. \begin{array}{ll} \dfrac{\partial u}{\partial y} = 0 & \text{at } y = 0 \text{ (symmetry condition)}, \\[2mm] u = -1 + \beta(x) & \text{at } y = h \text{ (imposed wall velocity).} \end{array} \right\} \tag{2.5}$$

While the correct form of $\beta(x)$ should be determined based on clinical experiments, these quantitative data are not yet available, and we defer investigating a more realistic and clinical form of $\beta(x)$ for future studies. Here, we examine general effects of wall longitudinal motion on peristalsis, to do so we assume β is in the form of periodic Gaussian as follows:

$$\beta = \beta_0 + \sum_{m=-\infty}^{\infty} \beta_1 \exp \frac{-(kx - mk\lambda - \phi)^2}{2\beta_2^2}. \tag{2.6}$$

Here ϕ, β_1 and β_2 are parameters controlling phase, amplitude and width of β, respectively. Parameter β_0 is a constraint ensuring that the motion of the wall in the wave frame remains 2π-periodic in time (in the Lagrangian sense). Parameter $\beta_0(b, \beta_1, \beta_2)$ must be obtained such that the wall in the wave frame travels one wavelength in one waveperiod, i.e. to satisfy

$$\int_0^{\omega T = 2\pi} u(x, y = h) \, dt = -k\lambda = -2\pi. \tag{2.7}$$

The summation in (2.6) is required to make β periodic. We find that for the range of β_2 considered in this study, it is sufficient to truncate the summation from $m = -5$ to 5. The form of β given in (2.6) is far from general but allows consideration of localized wall motion near the lumen extremas with phase lags.

2.2. *Flow kinematics*

The problem given by (2.4a,b) can be rewritten in terms of a stream function ψ (satisfying $u = \partial\psi/\partial y$, $v = -\partial\psi/\partial x$) as

$$\frac{\partial^4 \psi}{\partial y^4} = 0. \tag{2.8}$$

Boundary conditions given by (2.5) can also be expressed in terms of the stream function as

$$\left. \begin{array}{ll} \dfrac{\partial^2 \psi}{\partial y^2} = 0 & \text{at } y = 0, \\[2mm] \dfrac{\partial \psi}{\partial y} = -1 + \beta(x) & \text{at } y = h. \end{array} \right\} \tag{2.9}$$

The two remaining conditions needed to solve (2.8) can be obtained by noting that in the wave frame both planes $y = 0$ and $y = h$ are streamlines and the volume flow rate q is

constant at all cross-sections:

$$\begin{rcases} \psi = 0 & \text{at } y = 0, \\ \psi = q & \text{at } y = h. \end{rcases} \tag{2.10}$$

Solving (2.8)–(2.10) gives u and v as

$$u = \frac{3}{2}\frac{h(1-\beta)+q}{h}\left[1 - \left(\frac{y}{h}\right)^2\right] - (1-\beta), \tag{2.11}$$

$$v = \frac{h\beta' - h'(1-\beta)}{2}\frac{y}{h}\left[3 - \left(\frac{y}{h}\right)^2\right] - \frac{3}{2}\frac{h(1-\beta)+q}{h}\frac{y}{h}h'\left(\frac{y}{h} - 1\right)^2 - y\beta', \tag{2.12}$$

where the primes denote derivative with respect to x. An example of longitudinal velocity u for $\beta = 0$ – Shapiro *et al.* (1969) case – is shown in Appendix D, figure 13. The parabolic, Poiseuille type flow can be seen in the figure.

2.3. *Pressure-flow characteristics*

Considering that the peristaltic wave acts as a pump (i.e. working on the fluid to increase its pressure), two quantities of practical interest are the time-mean volume flow rate at each cross-section $\bar{Q}$, which measures the net volume flow or mean discharge rate (per lumen width), see Shapiro *et al.* (1969) for derivation, and the pressure rise per wavelength, Δp_λ:

$$\bar{Q} = q + 1, \tag{2.13}$$

$$\Delta p_\lambda = \int_0^{k\lambda = 2\pi} \frac{\mathrm{d}p}{\mathrm{d}x}\,\mathrm{d}x, \tag{2.14}$$

where $\mathrm{d}p/\mathrm{d}x = \partial p/\partial x$ can be obtained from (2.4a,b) and (2.11) as

$$\frac{\mathrm{d}p}{\mathrm{d}x} = \frac{-3}{h^3}[q + (1 - \beta)h]. \tag{2.15}$$

For complete lumen closure (i.e. $b = 1$), $\bar{Q} = 1$ and the peristaltic wave acts as a positive-displacement pump while, for no net flow, $\bar{Q} = 0$.

As is evident from (2.15) and consistent with Shapiro *et al.* (1969), due to the low-Reynolds-number assumption employed in this study, Δp_λ has a linear relationship with $\bar{Q}$; see figure 14(*a*) in Appendix D. Also, as noted by Shapiro *et al.* (1969), this linear relationship can be characterized by horizontal and vertical intercepts of these curves with the following physical significance.

(i) Vertical intercepts with $\bar{Q} = 0$ are at Δp_λ^0 and indicate a pressure rise per wavelength for zero time-mean flow that is similar to when there is a blockage in the ureter or if the pressure difference between the bladder and the kidney are such that the net flow is zero.

(ii) Horizontal intercepts with $\Delta p_\lambda = 0$ are at $\bar{Q}_0$ and indicate a time-mean flow for a zero pressure rise per wavelength. At this flow rate the peristaltic wave is not doing useful work and flow is not controlled by the peristalsis. Under such conditions, depending on differential pressure between the kidneys and bladder, we might have no flow, forward flow or backward flow. In these situations, all the work done by the peristaltic wave will be converted to heat by viscous dissipation.

The above intercepts mark the range where the peristalsis acts as a pump, defined as the range of volume flow rates where mean flow is in the direction of the pressure rise per wavelength – non-negative $\bar{Q}$ and non-negative Δp_λ in figure 14(a) in Appendix D – i.e. $0 \leq \bar{Q} \leq \bar{Q}_0$. Consistent with similar works in the literature (Shapiro *et al.* 1969; Liron 1976), the peristalsis activity in this range is the focus here. For convenience, $\bar{Q}$ is normalized by its pumping range limit $\bar{Q}_0$ (see figure 14b in Appendix D):

$$\Gamma = \frac{\bar{Q}}{\bar{Q}_0}. \tag{2.16}$$

2.4. *Peristaltic reflux*

Peristaltic reflux is a topic of controversy in the literature. The debate is whether to use a Lagrangian description, advocated by Shapiro (1967), or an Eulerian description, promoted by Fung & Yih (1968), who argue that the Eulerian description gives the same result as the Lagrangian. Despite Shapiro & Jaffrin (1971) definitively showing the difference between the two descriptions and concluding that the Lagrangian description is the only correct one, the Eulerian description is still being commonly misused (Abd Elnaby & Haroun 2008; Jiménez-Lozano, Sen & Dunn 2009; Vahidi *et al.* 2011; Gad 2014; Hosseini *et al.* 2018). In such analysis, a time-mean velocity of less than zero is incorrectly identified as the criteria for peristaltic reflux. Furthermore, they predict reflux to happen in the centre of the lumen, which is not consistent with experimental results of Weinberg *et al.* (1971), showing reflux occurs near the wall. As shown previously (Shapiro *et al.* 1969; Takabatake & Ayukawa 1982) and in this study, peristaltic reflux can happen even when $\bar{Q} > 0$. Therefore, consistent with Shapiro *et al.* (1969), Shapiro & Jaffrin (1971), Takabatake & Ayukawa (1982), we define peristaltic reflux as retrograde motion of fluid particles, resulting in a net backward displacement of more than one wavelength over one waveperiod. The quantity of interest becomes the trajectories of fluid particles over one waveperiod, which can be obtained by solving an initial value problem given by

$$\frac{\mathrm{D}x}{\mathrm{D}t} = u, \quad \frac{\mathrm{D}y}{\mathrm{D}t} = v, \tag{2.17a,b}$$

where $\mathrm{D}/\mathrm{D}t$ is the total derivative and u and v are given by (2.11) and (2.12), respectively. The particle trajectories in the laboratory frame can be simply obtained by the coordinate transformation given in (2.3), i.e. $X = x + t$, $Y = y$. Examples of these trajectories showing refluxing and non-refluxing fluid particles, based on the above definition, are shown in figures 2(a) and 2(b) in the wave and laboratory frames, respectively. Note that the fluid particle starting closer to the wall refluxes while the fluid particle closer to the lumen centre does not. The corresponding animation of particle trajectories of figure 2(b) is shown in supplementary movie 1 available at https://doi.org/10.1017/jfm.2023.363. As evident in figure 2, the wave and particle periods are not the same. In the above figures, parameters $b = 0.8$ and $q = -0.7$ are chosen as an example case and are based on clinical expertise and anatomical measurements (see § 4 for more detail) and, unless stated otherwise, the same parameters are used for the remainder of the paper.

In light of the above discussion, a more rigorous criteria for peristaltic reflux can be defined based on the mean velocity of the fluid particles over one waveperiod ($\omega T = 2\pi$). The mean velocity of fluid particles $\bar{u}$ (or $\bar{U}$ in the laboratory frame) can be obtained from
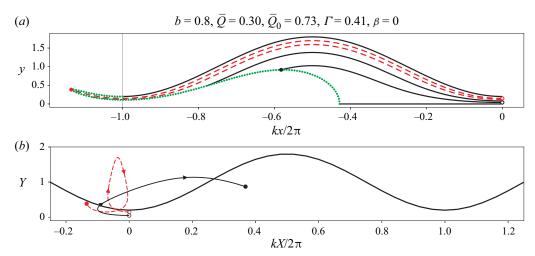
Figure 2. Example peristaltic reflux illustration. (*a*) Fluid pathlines are shown starting at $kx/2\pi = 0$ over one waveperiod ($0 < \omega t/2\pi < 1$) in the wave frame. The refluxing pathlines are shown as red dashed lines. The timeline originally vertically spanning the small gap at $kx/2\pi = 0$ is shown with a green dotted line at $\omega t/2\pi = 1$. (*b*) Two examples of pathlines in the laboratory frame starting at $kX/2\pi = 0$, $Y = 0.15$ (with net negative displacement, i.e. refluxing) and $kX/2\pi = 0$, $Y = 0.05$ (with net positive displacement, i.e. not refluxing). The associated particles in (*b*) are marked in (*a*) as well. The empty circles show initial locations while the filled circles are showing locations at the end of one waveperiod. The results are shown for $\beta = 0$, i.e. no wall longitudinal motion. The wall in (*b*), i.e. in the lab frame, translates and is shown at $\omega t/2\pi = 1$. The corresponding animation of (*b*) is shown in supplementary movie 1.

the horizontal motion of particles over one waveperiod Δx_λ as

$$\bar{u} = \frac{\Delta x_\lambda}{2\pi}, \quad \bar{U} = \bar{u} + 1. \tag{2.18a,b}$$

Mean velocities of $\bar{u} < -1$ in the wave frame (or $\bar{U} < 0$ in the laboratory frame) indicate fluid particles with a net backward motion of more than one wavelength over one waveperiod, i.e. refluxing condition, this is shown in figure 3. Therefore, the range of refluxing flow rates Γ_r can be defined as

$$\Gamma_r = \{\Gamma \in (0, 1) \mid \bar{U}(\Gamma) < 0\}. \tag{2.19}$$

2.5. *Reflux quantification*

Consistent with Takabatake & Ayukawa (1982), since we use the waveperiod not the particle period for calculating the mean velocity of figure 3, we can integrate $\bar{U}$ with respect to Y in the refluxing range to calculate the time-mean backward (i.e. refluxing) volume flow rate per unit width in the out-of-plane direction:

$$\bar{Q}_r = \int_{\bar{U}<0} \bar{U} \, dY. \tag{2.20}$$

Similarly, the time-mean forward (non-refluxing) volume flow rate $\bar{Q}_{nr}$ can be calculated as

$$\bar{Q}_{nr} = \int_{\bar{U}>0} \bar{U} \, dY. \tag{2.21}$$

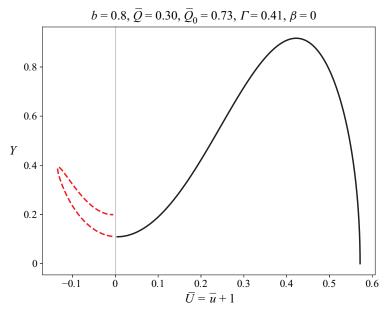$$b = 0.8, \bar{Q} = 0.30, \bar{Q}_0 = 0.73, \Gamma = 0.41, \beta = 0$$

Figure 3. Reflux criteria. Average longitudinal velocity of fluid particles at $kX/2\pi = 0$ over one waveperiod ($0 < \omega t/2\pi < 1$) in the laboratory frame. The dashed red line is showing refluxing fluid particles. The forward and backward (reflux) time-mean volume flow rate can be calculated by integrating $\bar{U}$ with respect to Y for $\bar{U} > 0$ and $\bar{U} < 0$, respectively. This figure is identical to the timeline of figure 2(a) at $\omega t/2\pi = 1$ (green dotted line), albeit at a different scale.

The flow rates Q_r and Q_{nr} are represented by the areas enclosed by the red dashed line bounded by $\bar{U} = 0$, and by the solid curve bounded by $Y = 0$ and $\bar{U} = 0$, respectively. The algebraic sum of the refluxing and non-refluxing flow rates gives the net time-mean flow rate $\bar{Q} = \bar{Q}_r + \bar{Q}_{nr}$. Lastly, the reflux fraction $\mathcal{X}$ can be defined as the ratio of magnitudes of the refluxing to net volume flow rates, i.e.

$$\mathcal{X} = \frac{|\bar{Q}_r|}{\bar{Q}}. \tag{2.22}$$

2.6. *Efficiency*

In the peristaltic wave pumping range ($0 \leq \Gamma \leq 1$), the mechanical efficiency E can be obtained based on its common definition in pumping machinery as

$$E = \frac{\bar{Q}\Delta p_\lambda}{\bar{W}}, \tag{2.23}$$

where $\bar{Q}\Delta p_\lambda$ is the useful pumping power and $\bar{W}$ is the mean rate of wall mechanical work, both per wavelength and per unit width (Shapiro *et al.* 1969; Liron 1976). In the above equation $\bar{W}$ can be calculated by noting that it is the sum of the rate of useful pumping power ($\bar{Q}\Delta p_\lambda$) and viscous dissipation D:

$$\bar{W} = \bar{Q}\Delta p_\lambda + D, \tag{2.24}$$

964 A30-9

where D, based on the small slope approximation, is

$$D = \int_0^{2\pi} \int_0^h \left(\frac{\mathrm{d}p}{\mathrm{d}x}y\right)^2 \, \mathrm{d}y \, \mathrm{d}x. \qquad (2.25)$$

We note that efficiencies outside this pumping range (where $\bar{W}$ changes sign) have some anomalies that we do not yet understand. Peristaltic efficiency and reflux fraction in the pumping range, calculated numerically with (2.23)–(2.25), and (2.20)–(2.22), are plotted in figures 4(*a*) and 4(*b*), respectively for $\beta = 0$, i.e. the Shapiro *et al.* (1969) case. For comparison purposes, the Shapiro *et al.* (1969) results – their (17) and (51) for efficiency and reflux fraction, respectively – are overlaid on top of the results obtained here.

The spatial resolution for numerical integrations involved in (2.23) is $\Delta x = \Delta y/h = 0.01$. The ordinary differential equation (2.17*a,b*) for reflux quantification (2.20), on the other hand, is solved with a relative tolerance of 10^{-5} and spatial resolution of $\Delta y/h = 0.01$. The average error for efficiency compared with the closed-form solution of Shapiro *et al.* (1969), independent of the peristaltic amplitude b, is of the order of $\sim 10^{-6}$. The closed-form solution of Shapiro *et al.* (1969) for the reflux fraction is an expansion for small b (see their figure 13, where they compare the closed-form solution to the more accurate numerical integration results). Therefore, for the reflux fraction, the numerical error is estimated with the solution for finer temporal and spatial resolutions (relative tolerance of 10^{-6} and $\Delta y/h = 0.005$). This numerical error is of the order of $\sim 10^{-5}$ for the largest b considered ($b = 0.8$) and it decreases for smaller peristaltic amplitudes ($\sim 10^{-8}$ for $b = 0.3, 0.5$).

In both figures the lines show Shapiro *et al.* (1969) results while the discrete points indicate the results obtained here. In figure 4(*a*) (i.e. efficiency curves) the range of refluxing Γ, obtained from (2.19), are marked with empty circles. Similarly, the range of refluxing Γ predicted by Shapiro *et al.* (1969) – their (47) – are indicated with dotted lines ending with a vertical bar. In figure 4(*b*) the additional horizontal dashed line, indicating an example for a critical reflux fraction $\mathcal{X}_c$, is also plotted. This is because, although not well understood, small amounts of peristaltic reflux can be harmless, especially if they are not accompanied by other abnormal conditions such as high bladder pressure, poor contractility or a UTI (Boyarsky & Labay 1981). Therefore, the more important quantity for clinical applications would be the reflux volume fraction. The critical reflux fraction, beyond which the peristaltic reflux becomes harmful, depends on clinical scenarios and varies on a case-by-case basis. In this study and as shown in figure 4(*b*), we choose the critical reflux fraction of $\mathcal{X}_c = 0.02$ as an example. The following important observations can be made from figure 4.

(i) In the absence of ureteral wall longitudinal motion, peristaltic reflux is common for flow rates within the pumping range.
(ii) Depending on the peristaltic amplitude, there is a minimum flow rate required for preventing peristaltic reflux. This minimum required flow rate increases with increasing peristaltic amplitude.
(iii) The reflux fraction increases with peristaltic amplitude.
(iv) As the net volume flow rate increases, the reflux fraction decreases and, depending on the peristaltic amplitude, can go to zero.
(v) As the net volume flow rate decreases, the reflux fraction increases and at the limit $\Gamma \to 0$ it goes to infinity. This is because while the net flow goes to zero, the backward flow remains finite.
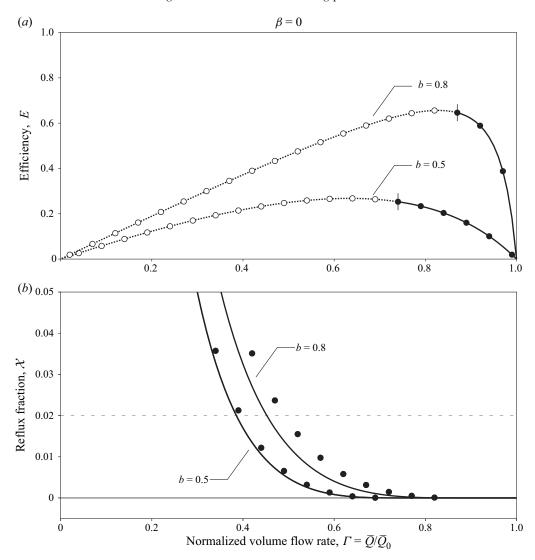
Figure 4. Peristaltic efficiency and reflux. (*a*) Pump efficiency and (*b*) reflux fraction plotted against normalized volume flow rate for two different peristaltic amplitudes $b = 0.5$ and 0.8. The results are obtained with $\beta = 0$ (without wall longitudinal motion). The lines show the results from the analytical model (Shapiro *et al.* 1969) – their (17) and (51) – while the discrete points are obtained with our numerical model. The refluxing conditions in (*a*) are shown with empty circles and dotted lines. The short vertical bar in (*a*) is the limit of reflux as predicted by the Shapiro *et al.* (1969) model (the minimum needed normalized volume flow rate to prevent reflux). The numerical and analytical solutions match for the case of $\beta = 0$ – the discrepancy in (*b*) is due to the expansion solution approximation employed by Shapiro *et al.* (1969). For clarity, the discrete points with zero reflux fractions are omitted in (*b*). In (*b*) the example critical reflux fraction $\mathcal{X}_c = 0.02$, described in the text, is shown with a dashed horizontal line as an example.

(vi) As the peristaltic amplitude increases ($b \to 1$), the maximum peristalsis efficiency increases but at the cost of an increase in the refluxing range and refluxing volume fractions.
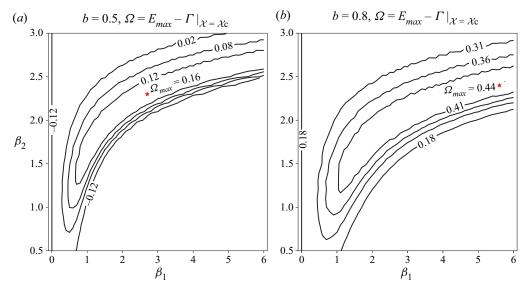
Figure 5. Optimization procedure for finding optimal parameters β_1 and β_2 for a combination of efficiency (E_{max}) and range of Γ where the peristaltic reflux fraction remains below its critical value ($\mathcal{X}_c = 0.02$ as an example in this study). Contour lines of objective function Ω given by (3.1) are plotted for β_1 and β_2 for peristaltic amplitudes of (a) $b = 0.5$ and (b) $b = 0.8$. Here $\beta_1 = 0$ recovers the Shapiro *et al.* (1969) case with $\Omega = -0.12$ and 0.18 for $b = 0.5$ and 0.8, respectively. The optimum parameters for $b = 0.5$ and 0.8 are found to be $\beta_1 = 2.7$, $\beta_2 = 2.3$ and $\beta_1 = 5.6$, $\beta_2 = 2.4$, respectively. Small jaggedness seen in the figure is due to numerical resolution of not only β_1 and β_2 but Γ (see figure 4). The resolution of Γ is of particular importance since it controls the numerical values of Ω in (3.1).

3. Effect of wall longitudinal motion

As mentioned earlier, while the correct form of wall longitudinal motion needs to be determined experimentally, in this study we assume it to be in the form of a periodic Gaussian given by (2.6). This form of β, through three parameters β_1, β_2 and ϕ, provides a general case for such a function. We first assume β is in-phase with the peristaltic wave, i.e. $\phi = \pi$, and parameters β_1 and β_2 are found using an optimization procedure based on an objective function Ω defined as

$$\Omega = E_{max} - w\Gamma|_{\mathcal{X}=\mathcal{X}_c}, \tag{3.1}$$

where $w > 0$ is the weight that we assume to be simply $w = 1$. The simple objective function Ω defined above is one of many forms, and is based on the notion that the peristaltic wave, while maintaining high efficiency, should result in zero or small reflux fractions ($\mathcal{X} < \mathcal{X}_c$). In doing so, it treats both peristaltic maximum efficiency and its reflux-prevention capability as equally important (since both quantities are normalized to vary between 0 and 1). The objective function would vary (in terms of its constituents, weights, linearity, etc.) for different clinical scenarios (e.g. high or low differential pressure between the bladder and kidney, UVJ deficiency, etc.).

The objective function Ω is evaluated on a grid of β_1 and β_2 ($0 \leq \beta_1 \leq 6, 0.5 \leq \beta_2 \leq 3$ with increments of 0.1 in each direction), and the corresponding contour lines are shown in figures 5(a) and 5(b) for $b = 0.5$ and 0.8, respectively. For $b = 0.5$, parameters $\beta_1 = 2.7$, $\beta_2 = 2.3$ result in an optimum $\Omega = 0.16$, while for $b = 0.8$, the optimum $\Omega = 0.44$ is achieved at $\beta_1 = 5.6$, $\beta_2 = 2.4$. This suggests that the ureteral wall longitudinal motion during peristalsis depends on the peristaltic amplitude, which is consistent with our own
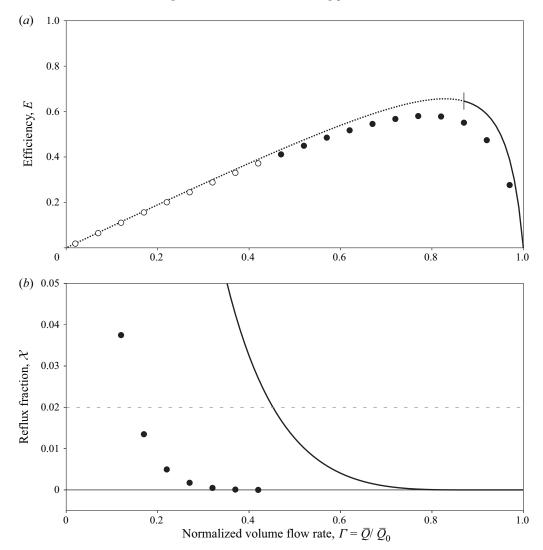
964 A30-12

Figure 6. Effect of wall longitudinal motion on peristalsis performance. (*a*) Peristaltic efficiency and (*b*) reflux fraction are plotted against Γ in the pumping range for the peristaltic amplitude of $b = 0.8$. The lines are showing the results associated with $\beta = 0$, i.e. the Shapiro *et al.* (1969) case, while the points are obtained with wall longitudinal motion, $\beta_1 = 5.6$, $\beta_2 = 2.4$ (optimum parameters obtained for the peristaltic amplitude of $b = 0.8$, figure 5). As in figure 4, the refluxing conditions in (*a*) are shown with a dotted line and empty circles. In (*b*) the discrete points with zero reflux fractions are omitted for clarity.

clinical observations. Additionally, the value of the objective function Ω increases with peristaltic amplitude, which implies that nearly full closure during the contraction phase of peristalsis is preferred; this is also consistent with our and other's observations, see Kiil (1973) for example. Lastly, although not shown here, varying the phase parameter ϕ slightly about π shows that the wall longitudinal motion is optimal when β is in-phase with h. Hence, the ureteral wall has maximum (positive) longitudinal velocity when the ureter is distended and minimum (negative) value when contracted.

$b = 0.8, \bar{Q} = 0.30, \bar{Q}_0 = 0.55, \Gamma = 0.55, \beta_1 = 5.6, \beta_2 = 2.4, \beta_0 = -0.55$
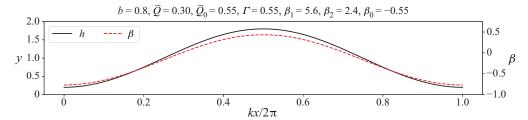

Figure 7. Longitudinal velocity of the wall. Left axis: lateral position of the wall y (2.2), black solid line. Right axis: longitudinal imposed velocity on the wall β (2.6), red dashed line.
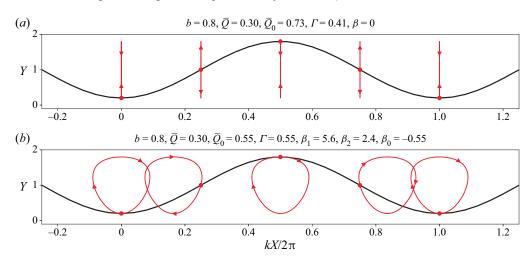

Figure 8. Wall longitudinal motion. Example trajectories of particles at $kX/2\pi = 0, 0.25, 0.5, 0.75$ and 1 on the wall over one waveperiod ($0 < \omega t/2\pi < 1$) (*a*) without longitudinal motion, i.e. $\beta = 0$, the Shapiro *et al.* (1969) case, and (*b*) with longitudinal motion ($\beta_1 = 5.6, \beta_2 = 2.4$). The trajectories are shown in the laboratory frame. The wave translates from left to right and is shown at $\omega t/2\pi = 1$. The corresponding animations are shown in supplementary movies 2 and 3.

For the remainder of this section and unless stated otherwise, parameters $\phi = \pi$, $\beta_1 = 5.6$ and $\beta_2 = 2.4$, the optimal parameters for peristaltic amplitude $b = 0.8$, are used to further illustrate the effect of wall longitudinal motion.

The effect of wall longitudinal motion on peristaltic performance is demonstrated in figure 6. More specifically, the peristaltic pumping efficiency and reflux fraction are plotted in figures 6(*a*) and 6(*b*), respectively. As shown in figure 6(*a*), while the efficiency remains almost at the same level as the case with no longitudinal motion ($\beta = 0$; lines), the refluxing range drops substantially from approximately $\Gamma < 0.9$ to $\Gamma < 0.45$. Similarly, as shown in figure 6(*b*), the minimum required Γ for $\mathcal{X} < \mathcal{X}_c = 0.02$ drops from approximately 0.5 to 0.15. Similar general effects have been observed for a peristaltic amplitude of $b = 0.5$; see figure 15 in Appendix D. These modelling results confirm that optimal longitudinal motion of the ureteral wall plays a substantial role in suppressing reflux, which needs to be experimentally verified.

The imposed wall longitudinal velocity β given by (2.6) along with the wall transverse coordinate h given by (2.2) are plotted in figure 7. As shown, function β obtained with the optimum parameters β_1 and β_2 appears to be linearly dependent on h. This is confirmed by calculating the Pearson correlation coefficient $r \approx 0.99$, indicating a simpler form of $\beta = \beta_0 + \beta_1 h$ is appropriate.

964 A30-14

(*a*) $b = 0.8$, $\overline{Q} = 0.30$, $\overline{Q}_0 = 0.55$, $\Gamma = 0.55$, $\beta_1 = 5.6$, $\beta_2 = 2.4$, $\beta_0 = -0.55$
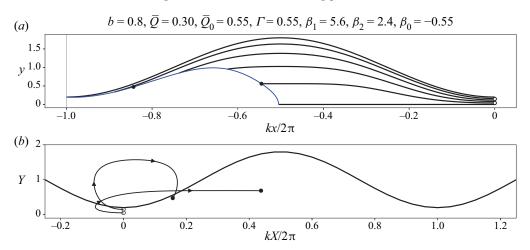

(*b*)

Figure 9. Ureteral wall longitudinal motion prevents peristaltic reflux. Compare this figure with its counterpart without wall longitudinal motion – $\beta = 0$, i.e. the Shapiro *et al.* (1969) case – in figure 2. The animation of (*b*) is shown in supplementary movie 4.
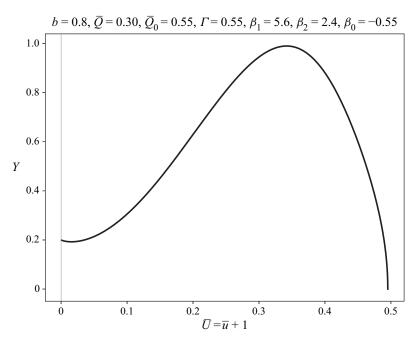
$b = 0.8$, $\overline{Q} = 0.30$, $\overline{Q}_0 = 0.55$, $\Gamma = 0.55$, $\beta_1 = 5.6$, $\beta_2 = 2.4$, $\beta_0 = -0.55$

$\overline{U} = \overline{u} + 1$

Figure 10. Ureteral wall longitudinal motion prevents peristaltic reflux. Compare this figure to its counterpart without wall longitudinal motion with $\beta = 0$, i.e. the Shapiro *et al.* (1969) case, in figure 3.

The longitudinal motion of the wall during one peristaltic wave is shown in figure 8. More specifically, the trajectories of particles on the wall during one waveperiod in the laboratory frame are shown for the case of $\beta = 0$, i.e. the Shapiro *et al.* (1969) case, and $\beta \neq 0$ in figures 8(*a*) and 8(*b*), respectively, with corresponding animations in supplementary movies 2 and 3. For the $\beta = 0$ case, the wall undergoes transverse motion only, while for the case of $\beta \neq 0$, the particles on the wall follow an 'egg'-shape, cyclic and closed-path motion.
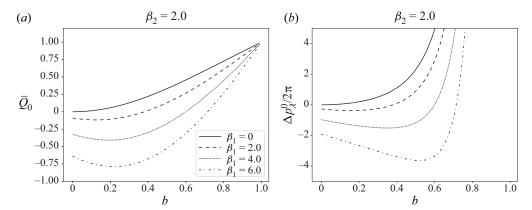
Figure 11. For peristalsis with wall longitudinal motion ($\beta > 0$) to act as a pump, larger peristaltic amplitudes are needed – peristalsis is no longer acting as a pump for negative $\bar{Q}_0$s and Δp_λ^0s in (*a*) and (*b*), respectively. Effect of β_1 on (*a*) volumetric flow rate for zero pressure rise per wavelength ($\bar{Q}_0$), and (*b*) pressure rise per wavelength for zero volume flow rate (Δp_λ^0). The results are obtained with $\beta_2 = 2.0$.

Figure 12. As β_2 increases, wall longitudinal motion becomes less effective, suggesting β might be a simple linear function of h. Effect of β_2 on (*a*) time-mean flow rate for zero pressure rise per wavelength ($\bar{Q}_0$), and (*b*) pressure rise per wavelength for zero time-mean flow rate (Δp_λ^0). The results are obtained with $\beta_1 = 0.5$.

Pathlines and trajectories of the same fluid particles shown in figure 2 for the case of $\beta = 0$ are replotted in figure 9 for the case with longitudinal motion. Pathlines (in the wave frame) are shown in figure 9(*a*), whereas the trajectories (in the laboratory frame) of fluid particles at $kX/2\pi = 0$, $Y = 0.15$ and $kX/2\pi = 0$, $Y = 0.05$ are plotted in figure 9(*b*). The animation corresponding to trajectories of figure 9(*b*) is shown in supplementary movie 4. By comparing these figures with their counterparts for the $\beta = 0$ case in figure 2, the effect of wall longitudinal motion on reflux becomes clearer. As shown, wall longitudinal motion causes a forward 'push' on fluid particles in the constricted area and close to the wall, and, therefore, depending on its magnitude, can overcome the net backward motion of such particles. This effect is also shown in figure 10, where the average longitudinal velocity $\bar{U}$ of fluid particles at $kX/2\pi = 0$ over one waveperiod in the laboratory frame are plotted. As shown in these figures, inclusion of longitudinal motion prevents peristaltic reflux for the case of $b = 0.8$ and $\bar{Q} = 0.3$. The effect of wall longitudinal motion on longitudinal velocity is shown in figure 16 in Appendix D.

964 A30-16

Lastly, the effect of parameter β_1 on $\bar{Q}_0$ and Δp_λ^0 are shown in figures 11(*a*) and 11(*b*), respectively. As shown in the figure, by introduction of longitudinal motion, peristalsis is no longer acting as a pump for all amplitudes – negative $\bar{Q}_0$s and Δp_λ^0s in figures 11(*a*) and 11(*b*), respectively. Additionally, as wall longitudinal motion increases, the minimum amplitude for peristalsis to act as a pump increases as well. This has an important implication, namely that the amplitude of wall longitudinal motion depends on peristaltic amplitude; the larger the peristaltic wave, the bigger the wall longitudinal motion. This important finding is consistent with our clinical observations. Similarly, a parametric study on β_2 and its effect on $\bar{Q}_0$ and Δp_λ^0 are shown in figures 12(*a*) and 12(*b*), respectively. As shown, as β_2 increases past its optimal value, wall longitudinal motion becomes less effective. This is because as β_2 increases, for β to remain periodic in space, β_0 becomes more negative; see (2.6) and (2.7). The increase in β_2 beyond its optimal value results in a net effect of flatter β with a mean value closer to zero. This further confirms that β can be more simply a linear function of h. The effect of parameters β_1 and β_2 on wall longitudinal velocity and motion is shown in Appendix D (figures 17–20).

4. Dimensional example

To signify the clinical importance of the findings of this study, we dimensionalize quantities of interest for the example parameters used in the preceding sections ($b = 0.8$, $\bar{Q} = 0.3$). A simple comparison between a two-dimensional planar model developed herein and more realistic axisymmetric geometry requires using a similar width and height for the ureter cross-section. Therefore, we assume that the width = height = $2\hat{a} = 3$ mm. Therefore, with

$$\hat{a} = 1.5 \text{ mm}, \quad \hat{b} = 1.2 \text{ mm}, \quad \hat{c} = 2 \text{ cm s}^{-1}, \quad \hat{\mu} = 0.001 \text{ Pa s}, \tag{4.1}$$

the net volume flow rate becomes $\hat{\bar{Q}} = 1.62$ mL min^{-1}, with 1.68 mL min^{-1} forward flow and 0.06 mL min^{-1} backward flow (reflux fraction of $\mathcal{X} = 0.04$). The pressure rise per wavelength for a zero time-mean flow, and time-mean flow for a zero pressure rise per wavelength become $\Delta \hat{p}_\lambda^0 = 2.13$ cmH$_2$O and $\hat{\bar{Q}}_0 = 3.93$ mL min^{-1}, respectively. Assuming three peristaltic waves are present in the ureter, the pressure differential between the bladder and kidneys (for zero time-mean flow) becomes 6.4 cmH$_2$O.

When considering wall longitudinal motion for the optimal $\beta_1 = 5.6$ and $\beta_2 = 2.4$ for the $b = 0.8$ case, the minimum and maximum wall longitudinal velocity become -1.54 cm s^{-1} and 0.88 cm s^{-1} during contraction and distension, respectively. Under this condition the refluxing flow rate becomes $\hat{\bar{Q}}_r = 0$ and the flow becomes unidirectional toward the bladder with $\hat{\bar{Q}}_{nr} = \hat{\bar{Q}} = 1.62$ mL min^{-1}. This dimensional example is in general agreement with a typical urinary tract physiology, as shown in Zheng *et al.* (2021).

5. Concluding remarks

This study, based on the classical lubrication model of peristalsis developed by Shapiro *et al.* (1969), for the first time considers the effect of wall longitudinal motion during peristalsis. We show that wall longitudinal motion is important for preventing or limiting peristaltic reflux. In doing so, we consider wall longitudinal velocity to be a general periodic Gaussian. We find a beneficial effect by choosing a specific form, however, further experimental observations and validations are needed to find an appropriate clinical form of such function. As an example, we show that for a normalized peristaltic amplitude

of $b = 0.8$, the minimum required flow rate to prevent reflux decreases from $\Gamma \approx 0.9$ to $\Gamma \approx 0.45$ when considering the wall longitudinal motion effect. Similarly, we show that the minimum flow rate to keep the reflux fraction below 2 % decreases from $\Gamma \approx 0.5$ to $\Gamma \approx 0.15$, again as an example for a peristaltic amplitude of $b = 0.8$. The results shown here indicate that the longitudinal velocity of the wall can be a function of wall lumen height. They also show wall longitudinal motion depends on peristaltic amplitude; higher peristaltic amplitudes come with larger longitudinal velocities. These results are in general agreement with clinical observations of ureteral peristalsis and highlight important gaps in previous studies that need further exploration. They augment our clinical understanding of normal and abnormal ureteral function, which is essential for understanding its disorders.

The two-dimensional model developed here will be used as a springboard to formulate more sophisticated models of peristalsis. We will find more clinically relevant non-sinusoidal peristalsis waveforms including those with wide and narrow boluses. Using operative videos, we will also determine a more realistic form of ureteral wall longitudinal motion based on particle tracking velocimetry of the ureter during peristalsis. While the considered two-dimensional planar flow qualitatively describes ureteral peristalsis clinical observations, it is not consistent with a circular cross-section of the ureter in the unconstricted region (Woodburne & Lapides 1972), which calls for a more appropriate axisymmetric model. Since during constriction the cross-section is no longer axisymmetric, we will combine the lubrication model with appropriate finite element simulations.

Author ORCIDs.
- Kourosh Kalayeh https://orcid.org/0000-0002-5254-6705;
- J. Brian Fowlkes https://orcid.org/0000-0002-4536-3919;
- Bryan S. Sack https://orcid.org/0000-0001-9576-0077;
- William W. Schultz https://orcid.org/0000-0001-7499-7868.

Appendix A. Note on solution development

Simplicity of the model without wall longitudinal motion allows Shapiro *et al.* (1969) to solve the problem analytically, but we have to solve the more general problem numerically. To do so, Python programming language (Python software foundation, Python language reference, version 3.9, available at http://www.python.org) and SciPy (Virtanen *et al.* 2020), NumPy (Harris *et al.* 2020) and Pandas (The Pandas Development Team 2022) open-source Python libraries for scientific and technical computing are used. All plots are generated with the Matplotlib open-source Python library (Hunter 2007). Additionally, unless stated otherwise, ordinary differential equations are solved with explicit Runge–Kutta method of order 5(4) (Dormand & Prince 1980) implemented

in SciPy `integrate.solve_ivp` method. Nonlinear equations are solved with Krylov method (Kelley 1995), implemented in SciPy `optimize.root` method. Numerical integrations are performed with the Gaussian quadrature rule, implemented in SciPy `integrate.quadrature` method.

Appendix B. Note on computation hardware

All the computations are run serially on The Great Lakes Slurm HPC cluster at the University of Michigan, Ann Arbor, MI, USA with a 3.0 GHz Intel Xeon Gold 6154 processor. The run execution time for obtaining efficiency and reflux fraction for a typical q, β_1 and β_2 (a typical discrete point in curves given in figure 6) is approximately 500 s.

Appendix C. Note on non-dimensionalization

As mentioned earlier, wave velocity $\hat{c}$, fluid viscosity $\hat{\mu}$ and lumen half-height $\hat{a}$ are chosen as characteristic quantities and the problem is non-dimensionalized by setting these quantities to unity, i.e.

$$\hat{L}_c = \hat{a}, \quad \hat{c}_c = \hat{c}, \quad \hat{\mu}_c = \hat{\mu}. \tag{C1a–c}$$

Using the above quantities, the normalized variables become

$$\left.\begin{array}{l} c = 1, \quad \mu = 1, \quad a = 1, \quad b = \hat{b}/\hat{a}, \quad h = \hat{h}/\hat{a}, \quad y = \hat{y}/\hat{a}, \\ k = 2\pi\hat{a}/\hat{\lambda}, \quad \omega = 2\pi\hat{a}/\hat{\lambda}, \quad kx = 2\pi\hat{x}/\hat{\lambda}, \quad \omega t = 2\pi\hat{t}\hat{c}/\hat{\lambda}, \\ p = \hat{p}k\hat{a}/2\pi\hat{\mu}\hat{c}, \quad q = \hat{q}/\hat{a}\hat{c}. \end{array}\right\} \tag{C2}$$

Appendix D. Supplementary figures

$b = 0.8, \bar{Q} = 0.30, \bar{Q}_0 = 0.73, \Gamma = 0.41, \beta = 0$
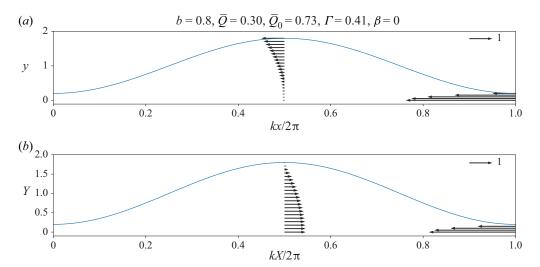
Figure 13. Parabolic velocity profile of Poiseuille type flow in the longitudinal direction in the peristaltic wave without wall longitudinal motion ($\beta = 0$) as predicted by Shapiro *et al.* (1969). The longitudinal velocity components u and U are plotted on two cross-sections in the (*a*) wave and (*b*) laboratory frames, respectively.
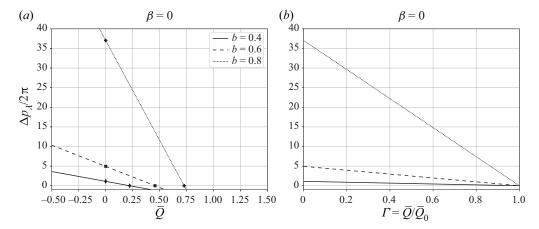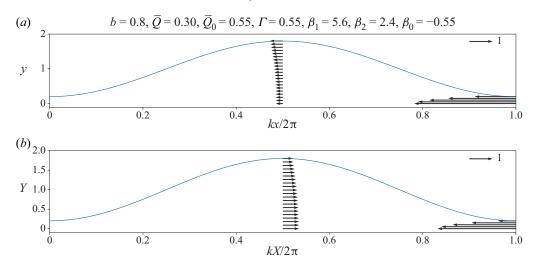
964 A30-19

Figure 14. Peristalsis pumping range. Pressure rise per wavelength Δp_λ plotted against (*a*) normalized time-mean flow rate, $\bar{Q}$, and (*b*) $\Gamma = \bar{Q}/\bar{Q}_0$ for $\beta = 0$, i.e. the Shapiro *et al.* (1969) case. In (*a*) the horizontal and vertical intercepts are marked by discrete points and show the flow rate at zero pressure rise per wavelength ($\bar{Q}_0$) and pressure rise per wavelength for zero flow rate (Δp_λ^0), respectively. Peristalsis pumping range is $0 \le \Gamma \le 1$ where the mean flow is in the direction of the pressure rise.

(*a*)

$$\beta_1 = 2.7, \ \beta_2 = 2.3$$

(*b*)

Figure 15. (*a*) Peristaltic pumping efficiency and (*b*) reflux fraction plotted against Γ for $b = 0.5$. The discrete points show results obtained for $\beta_1 = 2.7$, $\beta_2 = 2.3$, optimum parameters for $b = 0.5$, see figure 5, as lines for $\beta = 0$. As before, the refluxing condition in (*a*) is shown with a dotted line and empty circles. In (*b*) the discrete points with zero reflux volume fractions are omitted for clarity.

(a) $b = 0.8$, $\overline{Q} = 0.30$, $\overline{Q}_0 = 0.55$, $\Gamma = 0.55$, $\beta_1 = 5.6$, $\beta_2 = 2.4$, $\beta_0 = -0.55$

Figure 16. Parabolic velocity profile of Poiseuille type flow in the longitudinal direction in the peristaltic wave with wall longitudinal motion – longitudinal velocity of the wall is given by β in (2.6). The longitudinal velocity components u and U are plotted on two cross-sections in the (a) wave and (b) laboratory frames, respectively.
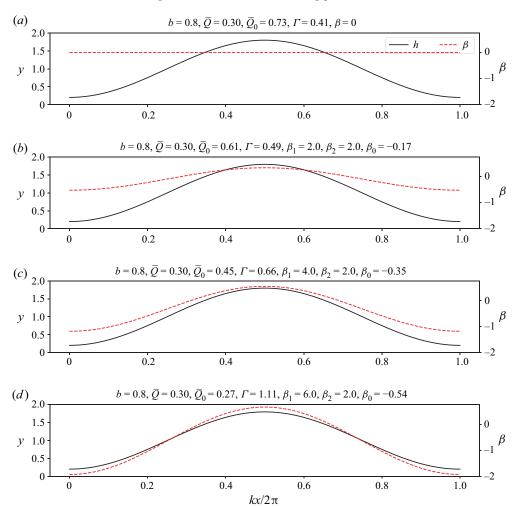
Figure 17. Effect of parameter β_1 on wall longitudinal velocity. Left axis: lateral position of the wall y, black solid line. Right axis: longitudinal imposed velocity on the wall β, red dashed line. Results are shown for (*a*) $\beta_1 = 0$ – the Shapiro *et al.* (1969) case, (*b*) $\beta_1 = 2.0$, (*c*) $\beta_1 = 4.0$ and (*d*) $\beta_1 = 6.0$. The results in (*b*)–(*d*) are obtained for $\beta_2 = 2.0$.
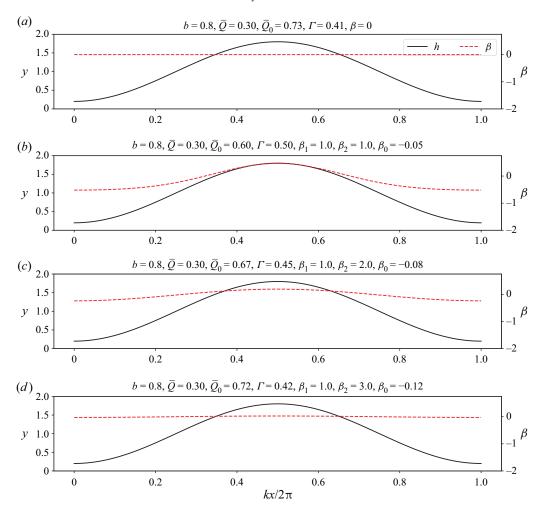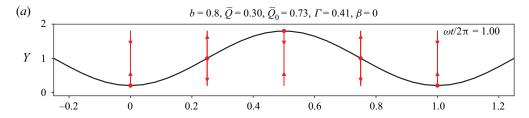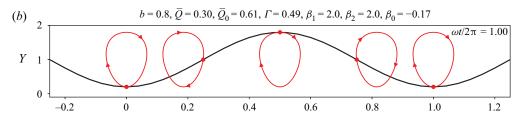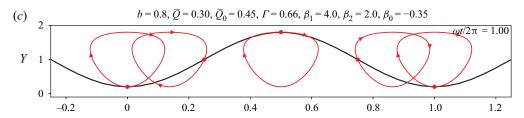
Figure 18. Effect of parameter β_2 on wall longitudinal velocity. Left axis: lateral position of the wall y, black solid line. Right axis: longitudinal imposed velocity on the wall β, red dashed line. Results are shown for (*a*) $\beta = 0$, (*b*) $\beta_2 = 1.0$, (*c*) $\beta_2 = 2.0$ and (*d*) $\beta_2 = 3.0$. The results in (*b*)–(*d*) are obtained for $\beta_1 = 1.0$.
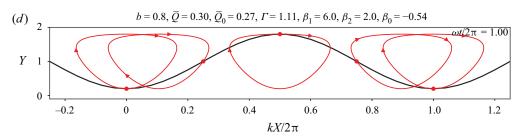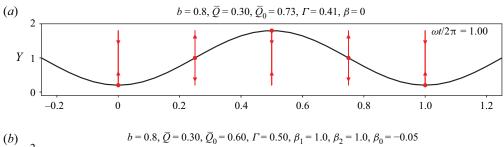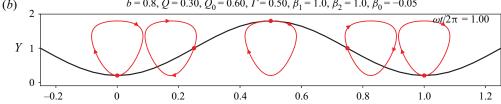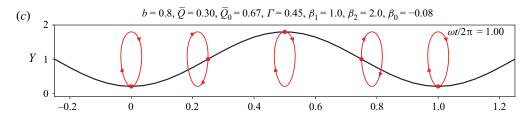
Figure 19. Effect of parameter β_1 on wall longitudinal motion. Example trajectories of particles at $kX/2\pi = 0, 0.25, 0.5, 0.75$ and 1 on the wall over one waveperiod ($\omega T/2\pi = 1$). Results are shown for (*a*) $\beta = 0$ – the Shapiro *et al.* (1969) case, (*b*) $\beta_1 = 2.0$, (*c*) $\beta_1 = 4.0$ and (*d*) $\beta_1 = 6.0$. The results in (*b*)–(*d*) are obtained for $\beta_2 = 2.0$.
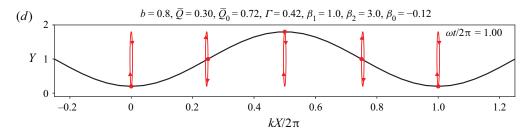
Figure 20. Effect of parameter β_2 on wall longitudinal motion. Example trajectories of particles at $kX/2\pi = 0, 0.25, 0.5, 0.75$ and 1 on the wall over one waveperiod ($\omega T/2\pi = 1$). Results are shown for (a) $\beta = 0$ – the Shapiro *et al.* (1969) case, (b) $\beta_2 = 1.0$, (c) $\beta_2 = 2.0$ and (d) $\beta_2 = 3.0$. The results in (b)–(d) are obtained for $\beta_1 = 1.0$.

REFERENCES

ABD ELNABY, M.A. & HAROUN, M.H. 2008 A new model for study the effect of wall properties on peristaltic transport of a viscous fluid. *Commun. Nonlinear Sci. Numer. Simul.* **13** (4), 752–762.

BOYARSKY, S. & LABAY, P. 1981 Principles of ureteral physiology. In *The Ureter* (ed. H. Bergman), pp. 71–104. Springer.

DORMAND, J.R. & PRINCE, P.J. 1980 A family of embedded Runge–Kutta formulae. *J. Comput. Appl. Maths* **6** (1), 19–26.

FUNG, Y.C. & YIH, C.S. 1968 Peristaltic transport. *J. Appl. Mech.* **35** (4), 669–675.

GAD, N.S. 2014 Effects of hall currents on peristaltic transport with compliant walls. *Appl. Maths Comput.* **235**, 546–554.

HARRIS, C.R., *et al.* 2020 Array programming with numpy. *Nature* **585** (7825), 357–362.

HOSSEINI, G., JI, C., XU, D., REZAIENIA, M.A., AVITAL, E., MUNJIZA, A., WILLIAMS, J.J.R. & GREEN, J.S.A. 2018 A computational model of ureteral peristalsis and an investigation into ureteral reflux. *Biomed. Engng Lett.* **8** (1), 117–125.

HUNTER, J.D. 2007 Matplotlib: a 2D graphics environment. *Comput. Sci. Engng* **9** (3), 90–95.

JAFFRIN, M.Y. & SHAPIRO, A.H. 1971 Peristaltic pumping. *Annu. Rev. Fluid Mech.* **3**, 13–37.

JIMÉNEZ-LOZANO, J., SEN, M. & DUNN, P.F. 2009 Particle motion in unsteady two-dimensional peristaltic flow with application to the ureter. *Phys. Rev. E Stat. Nonlinear Soft Matt. Phys.* **79** (4 Pt 1), 041901.

JÖRGENSEN, T.M. 1985 Dynamics of the urinary tract in longterm vesico-ureteric reflux and infravesical obstruction in pigs. IV. *Scand. J. Urol. Nephrol.* **19** (3), 193–202.

JÖRGENSEN, T.M. 1986 Pathogenetic factors in vesicoureteral reflux. *Neurourol. Urodyn.* **5** (2), 153–183.

JÖRGENSEN, T.M. & STÖDKILDE-JÖRGENSEN, H. 1985 Dynamics of the urinary tract during induced vesico-ureteric reflux in pigs. II. *Scand. J. Urol. Nephrol.* **19** (3), 173–182.

KALAYEH, K., FOWLKES, J.B., SCHULTZ, W.W. & SACK, B.S. 2020 Ureterovesical junction deformation during urine storage in the bladder and the effect on vesicoureteral reflux. *J. Biomech.* **113**, 110123.

KALAYEH, K., FOWLKES, J.B., SCHULTZ, W.W. & SACK, B.S. 2021 The 5:1 rule overestimates the needed tunnel length during ureteral reimplantation. *Neurourol. Urodyn.* **40** (1), 85–94.

KELLEY, C.T. 1995 *Iterative Methods for Linear and Nonlinear Equations*. Society for Industrial and Applied Mathematics.

KENI, L.G., HAYOZ, M.J., KHADER, S.M.A., HEGDE, P., PRAKASHINI, K., TAMAGAWA, M., SATISH SHENOY, B., HAMEED, B.M.Z. & ZUBER, M. 2021 Computational flow analysis of a single peristaltic wave propagation in the ureter. *Comput. Meth. Programs Biomed.* **210**, 106378.

KIIL, F. 1973 Urinary flow and ureteral peristalsis. In *Urodynamics*, pp. 57–70. Springer.

LI, M. & BRASSEUR, J.G. 1993 Non-steady peristaltic transport in finite-length tubes. *J. Fluid Mech.* **248**, 129–151.

LIRON, N. 1976 On peristaltic flow and its efficiency. *Bull. Math. Biol.* **38** (06), 573–596.

LYKOUDIS, P.S. & ROOS, R. 1970 The fluid mechanics of the ureter from a lubrication theory point of view. *J. Fluid Mech.* **43** (4), 661–674.

MACKINNON, K.J., FOOTE, J.W., WIGLESWORTH, F.W. & BLENNERHASSETT, J.B. 1970 The pathology of the adynamic distal ureteral segment. *J. Urol.* **103** (2), 134–137.

MANCHA SÁNCHEZ, E., GÓMEZ BLANCO, J.C., CRUZ CONTY, J.E.D.L., SÁNCHEZ MARGALLO, F.M., PAGADOR CARRASCO, J.B. & SORIA GÁLVEZ, F. 2020 Simplified model of ureteral peristalsis bolus using fluid structure interaction. In *Actas de las XXXIX Jornadas de Automática, Badajoz, 5–7 de Septiembre de 2018*. Universidade da Coruña. Servizo de Publicacións.

MANTON, M.J. 1975 Long-wavelength peristaltic pumping at low Reynolds number. *J. Fluid Mech.* **68** (3), 467–476.

OSMAN, F., NÁDASY, G.L., MONOS, E., NYIRÁD Y, P. & ROMICS, I. 2009 A novel videomicroscopic technique for studying rat ureteral peristalsis in vivo. *World J. Urol.* **27** (2), 265–270.

RAZAVI, S.E. & JOUYBAR, M. 2018 Fluid-structure interaction simulation of ureter with vesicoureteral reflux and primary obstructed megaureter. *Biomed. Mater. Engng* **29** (6), 821–837.

SHAPIRO, A.H. 1967 Pumping and retrograde diffusion in peristaltic waves. In *Proceedings of a Workshop on Ureteral Reflux in Children*, pp. 109–133. National Academy of Sciences.

SHAPIRO, A.H. & JAFFRIN, M.Y. 1971 Reflux in peristaltic pumping: is it determined by the Eulerian or Lagrangian mean velocity. *J. Appl. Mech.* **38** (4), 1060–1062.

SHAPIRO, A.H., JAFFRIN, M.Y. & WEINBERG, S.L. 1969 Peristaltic pumping with long wavelengths at low Reynolds number. *J. Fluid Mech.* **37** (4), 799–825.

SOM, S.K., BISWAS, G. & CHAKRABORTY, S. 2011 *Introduction to Fluid Mech & Fluid Machines*, 3rd edn. Tata McGraw-Hill Education.

TAKABATAKE, S. & AYUKAWA, K. 1982 Numerical study of two-dimensional peristaltic flows. *J. Fluid Mech.* **122** (1), 439–465.

THE PANDAS DEVELOPMENT TEAM 2022 Pandas-dev/pandas: Pandas. Zenodo.

VAHIDI, B., FATOURAEE, N., IMANPARAST, A. & MOGHADAM, A.N. 2011 A mathematical simulation of the ureter: effects of the model parameters on ureteral pressure/flow relations. *Trans. ASME J. Biomech. Engng* **133** (3), 031004.

VIRTANEN, P., *et al.* 2020 SciPy 1.0: fundamental algorithms for scientific computing in python. *Nat. Meth.* **17** (3), 261–272.

WEINBERG, S.L., ECKSTEIN, E.C. & SHAPIRO, A.H. 1971 An experimental study of peristaltic pumping. *J. Fluid Mech.* **49** (03), 461–481.

WEISS, R.M. 1978 Uretral function. *Urology* **12** (2), 114–133.

WOODBURNE, R.T. & LAPIDES, J. 1972 The ureteral lumen during peristalsis. *Am. J. Anat.* **133** (3), 255–258.

ZHENG, S., CARUGO, D., MOSAYYEBI, A., TURNEY, B., BURKHARD, F., LANGE, D., OBRIST, D., WATERS, S. & CLAVICA, F. 2021 Fluid mechanical modeling of the upper urinary tract. *WIREs Mech. Dis.* **13** (6), e1523.